Journal of ELECTRONIC MATERIALS, Vol. 44, No. 8, 2015
DOI: 10.1007/s11664-015-3727-3

Dielectric Dispersion, Diffuse Phase Transition, and Electrical Properties of BCT–BZT Ceramics Sintered at a Low-Temperature

YONGSHANG TIAN,[1] YANSHENG GONG,[1,2] DAWEI MENG,[1,3] YUANJIAN LI,[1] and BOYA KUANG[1]

1.—Faculty of Material Science and Chemistry, China University of Geosciences, Wuhan 430074, People's Republic of China. 2.—e-mail: gongysh@cug.edu.cn. 3.—e-mail: dwmeng@cug.edu.cn

Lead-free ceramics $0.50Ba_{0.9}Ca_{0.1}TiO_3$–$0.50BaTi_{1-x}Zr_xO_3$ (BCT–BZT) were prepared via sintering BCT and BZT nanoparticles, which were synthesized using a modified Pechini polymeric precursor method, at a low temperature of 1260°C. The relative densities of the ceramics prepared with different zirconium contents (x) were all above 95.3%, reaching a maximum of 97% when $x = 0.08$. X-ray diffraction results confirmed the onset of phase transformation from orthorhombic to rhombohedral symmetry with increasing zirconium contents, and the polymorphic phase transition was observed at $x = 0.10$. The dielectric dispersion, diffuse phase transition (DPT), and relaxor-like ferroelectric characteristics as a function of zirconium content were thoroughly studied. Optimum physical properties, remnant polarization (P_r) = 16.4 $\mu C/cm^2$, piezoelectric constant (d_{33}) = ~240 pC/N, and electromechanical coupling factor (k_p) = 0.22, were obtained at $x = 0.10$. The findings of the current DPT behavior study of BCT–BZT ceramics are believed to be insightful to the development of ferroelectric materials.

Key words: BCT–BZT ceramics, polymorphic phase transition, dielectric dispersion, diffuse phase transition

INTRODUCTION

Lead-based materials are widely used as sensors, actuators, acoustic emitters, filters, transducers, and capacitors owing to their excellent electrical properties.[1–3] However, those materials are potentially toxic owing to the generation of lead oxide during application, thereby presenting a health hazard to the environment and humans. Thus, developing lead-free materials as alternatives to lead-based materials is essential.[4,5] Research on lead-free materials includes $BaTiO_3$ (BT)-, $K_{0.5}Na_{0.5}NbO_3$ (KNN)-, $Bi_{0.5}Na_{0.5}TiO_3$ (BNT)-, and $BiFeO_3$ (BFO)-based systems.[6–11] Among all studied lead-free materials, BT-based materials have been historically used as piezoelectric devices because they feature no volatile elements, and have controllable sinterability and grain size. However, owing to their high permittivity and low piezoelectric properties, BT-based materials have been alternatively applied as dielectric devices.[1,12] In 2009, Liu and Ren demonstrated the existence of a morphotropic phase boundary (MPB) region in BT-based ceramics that was responsible for the development of piezoelectric properties which were comparable to those of lead-based ceramics.[13] Since then, BT-based ceramics have received increasing research interest.

BT-based ceramics have a perovskite structure (ABO_3), and the substitutions of the A sites by Ca and B sites by Zr are often used to improve their electrical properties.[14,15] Additionally, improved electrical properties by introducing rare earth elements and enhanced density by introducing metallic oxides as additives have been reported in the

(Received November 22, 2014; accepted March 4, 2015; published online April 11, 2015)

literature.[16,17] Among the electrical properties of BT-based ceramics studied, piezoelectric and ferroelectric properties have always been of major interest over the years.[18] The excellent properties observed in ferroelectric materials are attributed to high polarization rotation and polarization extension.[19] Furthermore, the study of ferroelectric diffusion phase transition (DPT), which may originate from polar nanoregions (PNRs) with various phase transition temperatures, and the relaxor-like ferroelectric characteristics of ferroelectric materials are very important for actual applications.[20,21] However, studies on the relationship between DPT and relaxor-like ferroelectric characteristics of the electrical properties of BT-based ceramics are rare.

BT-based ceramics are commonly obtained via sintering using conventional solid-state reactions at high temperatures (~1500°C), which can lead to inhomogeneous dispersion of the ingredients, resulting in crystal distortion, high internal stress, hard domain wall rotation, and inferior electrical properties.[22,23] In the present study, $0.5Ba_{0.8}Ca_{0.2}TiO_3$–$0.5BaTi_{1-x}Zr_xO_3$ (denoted as BCT–BZT) ceramics were prepared via sintering BCT and BZT nanoparticles, which were prepared using a modified Pechini polymeric precursor method, at a low temperature (1260°C), as reported in our previous study.[24] The phase transformation, DPT, relaxor-like ferroelectric characteristics, dielectric dispersion, and electrical properties of the ceramics were systematically studied. Additionally, the electrical properties around the polymorphic phase transition (PPT)/MPB-like region of the ceramics were investigated.

EXPERIMENTAL

$Ba_{0.8}Ca_{0.2}TiO_3$ (BCT) and $BaTi_{1-x}Zr_xO_3$ (BZT; x = 0, 0.03, 0.05, 0.08, 0.10, 0.12, 0.15, 0.20) nanoparticles were synthesized by a modified Pechini polymeric precursor method. The as-prepared BCT and BZT nanoparticles were stoichiometric mixed as 0.5BCT–0.5BZT (BCT–BZT), and then dried at 200°C. The BCT–BZT nanoparticles were then mixed with 2.5 wt.% polyvinyl alcohol solution binder, and uniaxially pressed into discs of 20 mm in diameter and ~1.5 mm in thickness at 150 MPa. Following burn-out of polyvinyl alcohol at 650°C, the resulting materials were finally sintered at 1260°C for 5 h in air to obtain the final ceramics. For the electrode preparation, the samples were polished, both sides of the polished discs were silver-painted, and then annealed at 570°C for 15 min for subsequent dielectric measurements. Then, the samples were polarized in a silicone oil bath under a direct-current electric field of 25 kV/cm at 25°C for ~40 min.

The crystal structure of the ceramics was investigated by x-ray diffraction (XRD; X'Pert PRO) using Cu Kα radiation at a 2θ scanning rate of 0.05°/s at room temperature at 40 kV and 40 mA. Field-emission scanning electron microscopy (FESEM; SUV-1080) was used to analyze the fractured microstructures, which were treated using a thermal etching process (1050°C, 15 min in atmosphere) followed by coating with Au for 160 s under vacuum. The density of the prepared materials was determined based on the Archimedes immersion principle using a precision electronic balance (ED-124S). The relative permittivity (ε_r) and loss tangent (tan δ) were determined using a precision LCR meter (TH-2819). A radiant precision workstation was carried to investigate polarization–electric field (P–E) hysteresis loops. The electromechanical coupling (k_p) and mechanical quality (Q_m) factors were calculated by the resonance–antiresonance method on a precision impedance analyzer (Agilent-4292A). A piezo-d_{33} quasi-static meter (ZJ-3A) was used to determine the piezoelectric constant (d_{33}).

RESULTS AND DISCUSSION

Figure 1 shows the XRD patterns of the BCT–BZT ceramics prepared with different zirconium contents (x). All the samples had a pure perovskite structure (ABO_3) without secondary phases, suggesting that zirconium was successfully impregnated into the ABO_3 lattice to form a solid solution in the BCT–BZT ceramics. The sharp diffraction peaks are indicative of the high crystallinity of the samples sintered at 1260°C. As observed in Fig. 1a, the intensity and position of the main diffraction peaks remained mostly unchanged with increasing x values. However, it could be observed that the diffraction peaks first receded and then were enhanced in the enlarged XRD patterns (Fig. 1b) with the addition of zirconium, which was associated with an evolvement of phase transition.[25] Additionally, the diffraction peak shifted monotonically to low 2θ angles with increasing x values in Fig. 1b, which was due to the substitution of Ti^{4+} (ionic radius

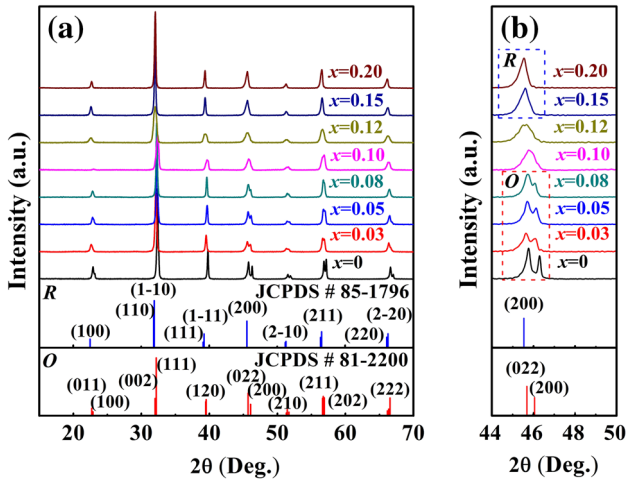

Fig. 1. XRD patterns (a) and selected enlarged regions of 44°–50° (b) of BCT–BZT ceramics with various zirconium contents (x).

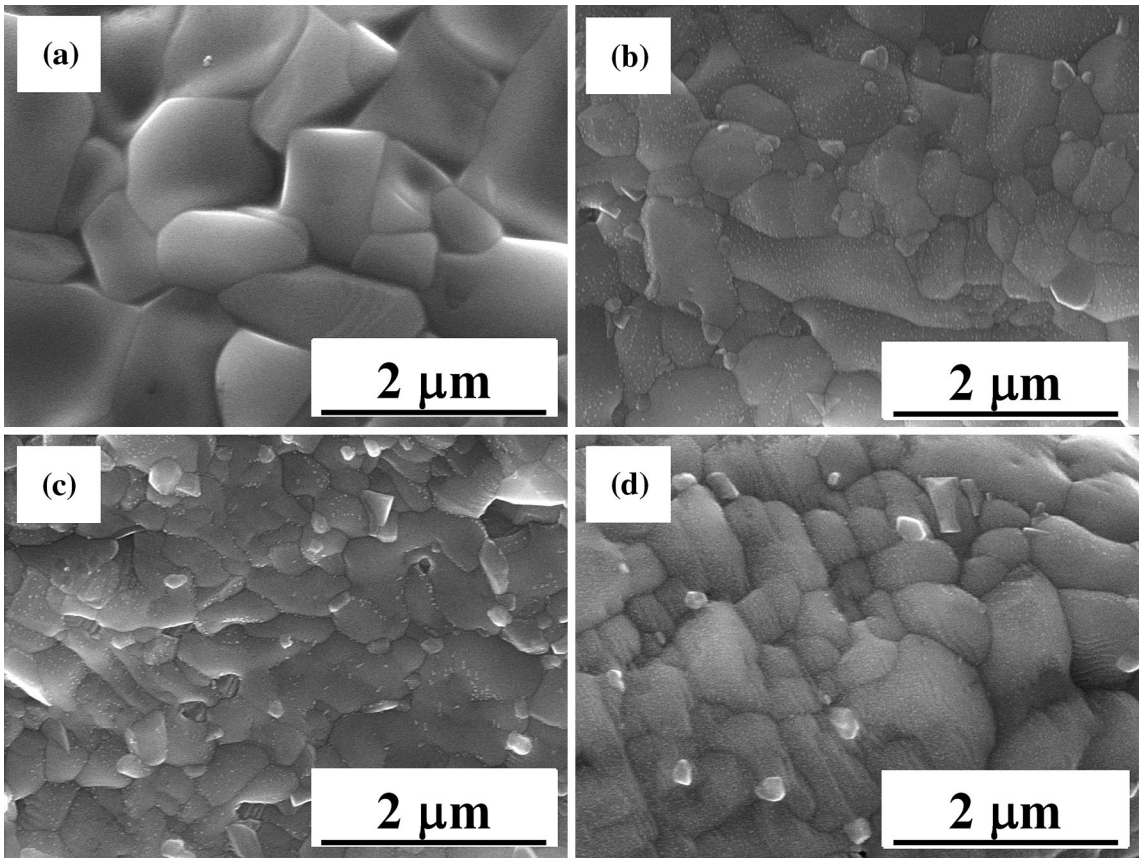

Fig. 2. FESEM images of BCT–BZT ceramics with zirconium contents (x) at (a) 0; (b) 0.05; (c) 0.10; and (d) 0.15.

$\sim$0.0605 nm) with Zr^{4+} (ionic radius 0.072 nm) in the ABO_3 structure.[26] As observed in Fig. 1b, the unique splitting (022) and (200) diffraction peaks at $\sim$46° of orthorhombic (O) symmetry (JCPDS # 81-2200) gradually merged into (200) diffraction peak of rhombohedral (R) symmetry (JCPDS # 85-1796) with increasing x values.[27] Thus, the O phase was observed at $0 < x < 0.08$, whereas the R phase was detected at $0.15 < x < 0.20$. Both the O and R phases were observed in the intermediate x range of 0.10–0.12. These results confirmed that the phase transition of the BCT–BZT ceramics was instigated by the distortion of the crystal lattice with increasing zirconium contents.[28]

The FESEM images of the BCT–BZT ceramics prepared with different zirconium content (x) are shown in Fig. 2. All the samples featured a dense microstructure, indicating that sintering at a low temperature (1260°C in this study) was effective. The average grain size of the samples prepared with varying x values was within 2 μm, which was considerably smaller than the literature value obtained from the conventional solid state reaction method.[29,30] The smaller grain size is believed to result in a relatively low permittivity.[31] Fine grain sizes with large grain boundary volumes may alter the fine balance between the long-range and short-range forces, resulting in a relaxor state in the ceramics.[31] Furthermore, the distortion of the grain and the presence of the ill-defined grain boundary were associated with the solubility limit of zirconium in BCT–BZT structure in the presence of excess zirconium content.

Figure 3 shows the density and relative density values of the BCT–BZT ceramics prepared with different zirconium contents (x) and sintered at 1260°C. The density of the ceramics first increased and then decreased with increasing x values. The maximum density of 5.75 g/cm^3 $\pm$ 0.01 g/cm^3 (relative density of $\sim$97%) was obtained at $x = 0.08$, and all the relative densities were above 95.3%, confirming the high level of densification in the ceramics sintered at a relatively low temperature. A high level of densification was always accompanied with low porosity and large domain size, resulting in low dielectric losses and weak pinching effects in the domain wall that were expected to result in outstanding dielectric properties and low mechanical quality factor (Q_m).[32–34] The increasing density of the ceramics prepared with increasing x values ($x < 0.08$) was attributed to the replacement of Ti by heavier atom mass Zr in the ABO_3 structure. Excessive addition of zirconium ($x > 0.10$) led to lattice expansion and distortion that reduced the level of densification of the BCT–BZT ceramics, as consistent with the above results.

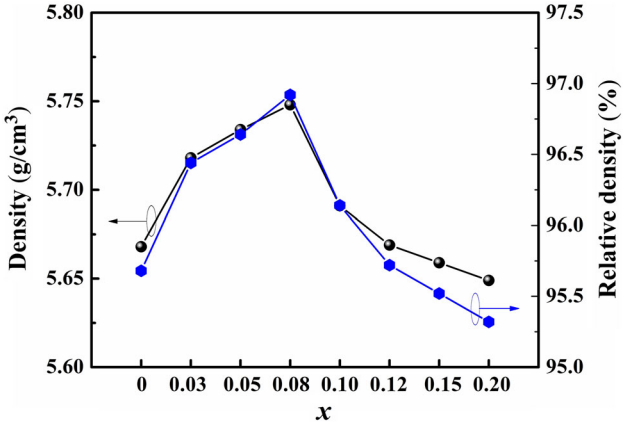

Fig. 3. The density and relative density of BCT–BZT ceramics with various zirconium contents (x).

Figure 4 shows the temperature dependence of relative permittivity (ε_r) and loss tangent (tan δ) of the BCT–BZT ceramics prepared with different zirconium contents (x) assessed at a frequency of 10 kHz. As observed in Fig. 4b, T_C increased subtly, then an obvious decrease was observed together with broadening of the dielectric peak with further increases in the x value. The obtained result was associated with the disordered crystal structure including compositional disorder and PNRs. Similar results were also reported by Dong et al.[26] and Yu et al.[35] The inset in Fig. 4a shows the enlarged regions of ε_r as a function of temperature from 25°C to 55°C. The broad dielectric peaks were attributed to the orthorhombic-to-tetragonal phase transition (T_{O-T}). The temperature at which the orthorhombic-to-tetragonal phase transition occurred (T_{O-T}) shifted to higher values with increasing zirconium contents. Furthermore, the observed merging of the T_{O-T} and T_C peaks was related to the pinching effect for the phase transition, which could improve the piezoelectric properties.[25,30] As T_{O-T} shifted to a higher value, the O phase became more predominant in the ceramics. Tan δ of the BCT–BZT ceramics in Fig. 4c was ~0.02 when assessed at 10 kHz, suggesting the presence of minimal crystal defects in the samples. Furthermore, the T_{O-T} and T_C peaks were clearly observed in tan δ–T curves, which could help to determine the phase transformation and the diffused characteristic of the ceramics.

The frequency dispersion of the BCT–BZT ceramics prepared with different zirconium content (x) is shown in Fig. 5. The maximum permittivity and tan δ decreased, and the dielectric peak shifted to higher temperatures with increasing frequencies. The frequency dispersion and diffuse phase transition were enhanced with increasing x values, indicating that the diffused characteristic and relaxor-like ferroelectric properties were strengthened.[36,37] Tan δ of the BCT–BZT ceramics differed significantly at different zirconium contents and at

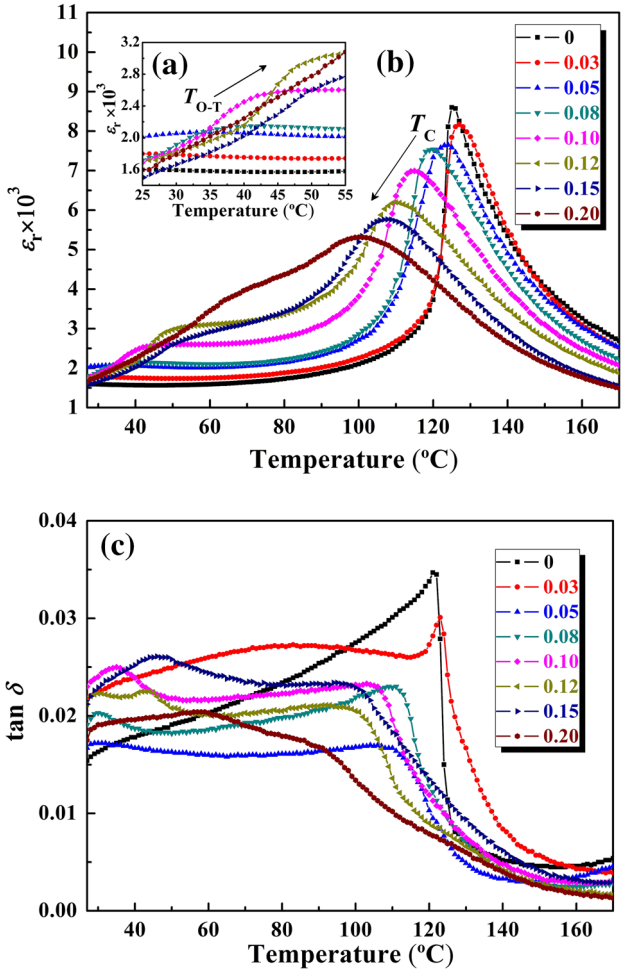

Fig. 4. Temperature dependence of relative permittivity (ε_r) (b) and loss tangent (tan δ) (c) of BCT–BZT ceramics. The inset in (a) shows the variation of ε_r at enlarged regions (25°C–55°C).

different frequency values ranging from 100 Hz to 10 kHz, thereby confirming the dependence of tan δ on the frequency and zirconium content. Moreover, the increased T_C was associated with the existence of a lower internal stress and constrained motion of the crystal surface under a higher frequency.[38] The higher relaxor-like ferroelectric characteristic of the ceramics with excess zirconium contents was attributed to the large mechanical impedance mismatch in the ABO_3 structure and high internal stress.[39]

To further study the degree of dielectric dispersion and diffuse phase transition, the quantitative parameters were calculated. Variations of the dielectric constant in typical ferroelectric materials follow the Curie–Weiss law (Eq. 1) above T_C[40]:

$$\frac{1}{\varepsilon_r} = \frac{T - T_{CW}}{C}, \quad (1)$$

where ε_r is the relative permittivity; T_{CW} is the Curie–Weiss temperature; and C is the Curie–Weiss constant. Figure 6 shows the inverse permittivity

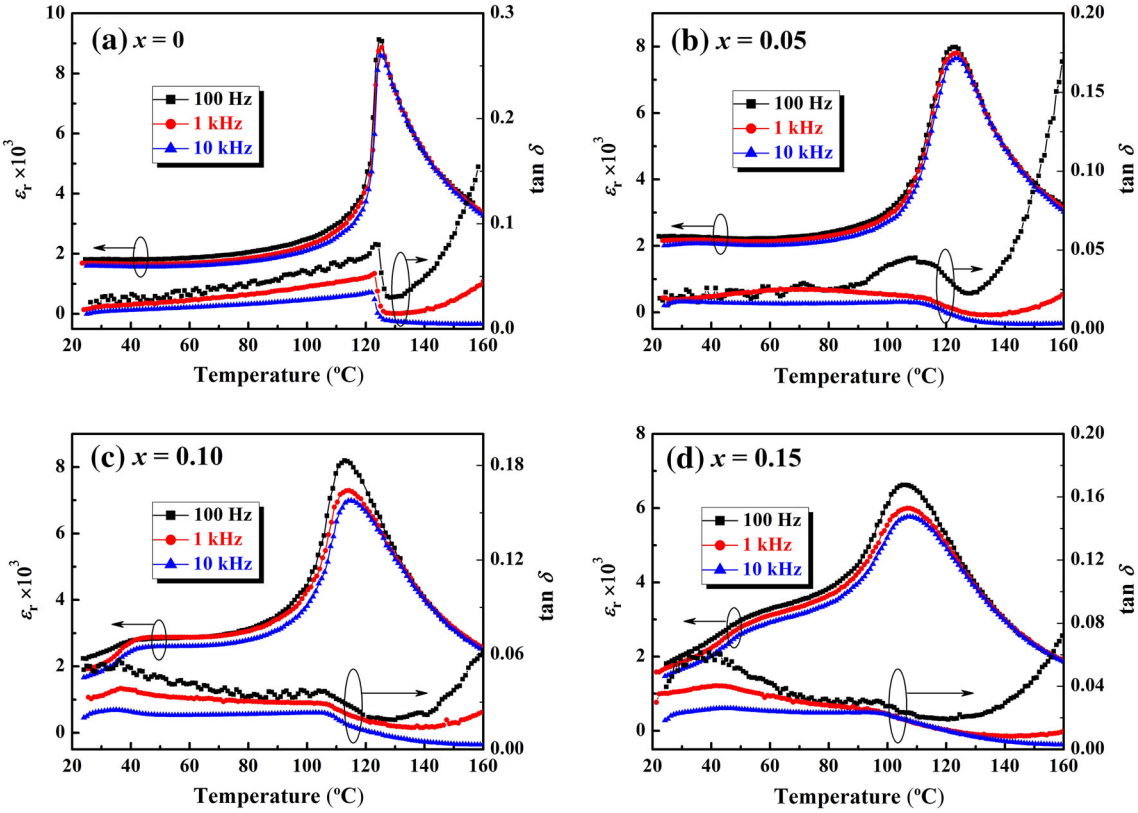

Fig. 5. Temperature dependence of relative permittivity (ε_r) of BCT–BZT ceramics with zirconium contents (x) of (a) 0; (b) 0.05; (c) 0.10; and (d) 0.15 under different measuring frequencies.

($10^4/\varepsilon_r$) as a function of temperature and the fit of the Curie–Weiss curve in the paraelectric region of the ceramics under 10 kHz using Eq. 2:

$$\Delta T_m = T_B - T_m, \tag{2}$$

where T_m is the temperature associated with the maximum permittivity; T_B corresponds to the temperature at which the permittivity starts to follow the Curie–Weiss law; and ΔT_m is the temperature deviation, which reveals the degree of diffusion.

The fitting results of the BCT–BZT ceramics at x = 0, 0.05, 0.10, and 0.15 are listed in Table I. As observed, ΔT_m increased from 20.6°C at x = 0°C to 34.9°C at x = 0.15, indicating that the diffuse phase transition and relaxor-like ferroelectric characteristics were enhanced with increasing zirconium contents. Moreover, C values of the samples were in the order of $\sim 10^5$, suggesting that the high-temperature paraelectric phase was driven by a displacive transition.[41] The C value decreased with increasing x values that also indicated that the relaxor-like ferroelectric characteristics were enhanced.[42]

The degree of relaxor-like ferroelectric characteristics and the ferroelectric diffuseness of the BCT–BZT ceramics were investigated by a modified Curie–Weiss law (Eq. 3)[43]:

$$\frac{1}{\varepsilon_r} - \frac{1}{\varepsilon_m} = \frac{(T - T_m)^\gamma}{C'}, \tag{3}$$

where ε_m is the maximum relative permittivity; C' is the modified Curie–Weiss constant; and γ is the degree of the diffuseness exponent. Parameter γ is calculated from the slope of the graph of $\ln(1/\varepsilon_r - 1/\varepsilon_m)$ versus $\ln(T - T_m)$. The obtained γ value was between 1 (normal ferroelectric) and 2 (typical relaxor ferroelectric). The γ values of the BCT–BZT ceramics at x = 0, 0.05, 0.10, and 0.15 under 10 kHz are shown in Fig. 7. The value of γ increased from 1.235 (x = 0) to 1.792 (x = 0.15), indicating that the diffuseness of the ceramics was enhanced upon the addition of zirconium, and this result was consistent with the above analysis and the literature reports.[37,44,45] Furthermore, the enhanced diffuseness was associated with the compositional fluctuation and structural disordering in the ABO_3 structure site, causing a microscopic heterogeneity.[46]

Figure 8 shows the polarization–electric field (P–E) hysteresis loops of the BCT–BZT ceramics prepared with different zirconium contents (x). All the samples showed a typical saturated hysteresis loop under a direct-current electric field of 25 kV/cm. Variations of the remnant polarization (P_r) and coercive field (E_c) are shown in the inset figure

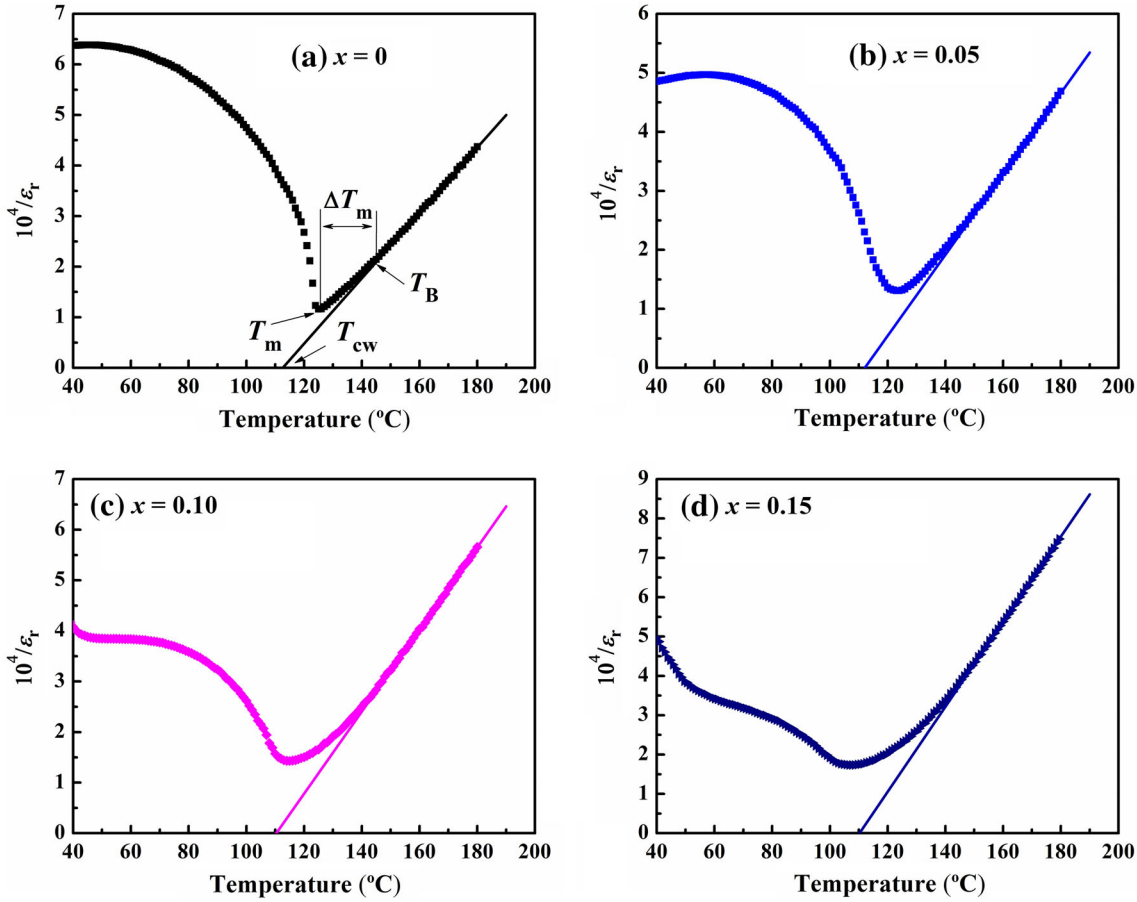

Fig. 6. Temperature dependences of inverse permittivity ($10^4/\varepsilon_r$) of BCT–BZT ceramics at 10 kHz with zirconium contents (x) of (a) 0; (b) 0.05; (c) 0.10; and (d) 0.15.

Table I. Temperature of the maximum permittivity (T_m); Curie–Weiss temperature (T_{CW}); temperature of the permittivity starts to follow Curie–Weiss law (T_B); temperature deviation (ΔT_m); and Curie–Weiss constant (C) for the BCT–BZT ceramics measured at 10 kHz

BCT–BZT	T_m (°C)	T_{cw} (°C)	T_B (°C)	ΔT_m (°C)	C ($\times 10^5$°C)
x = 0	124.9	112.7	145.5	20.6	1.547
x = 0.05	124.1	121.1	146.4	22.3	1.458
x = 0.10	115.3	110.5	141.7	26.4	1.232
x = 0.15	108.7	110.2	143.6	34.9	0.926

(Fig. 8a). P_r first increased with increasing x value, reaching a maximum value of 16.4 μC/cm^2 at x = 0.10, which was attributed to the coexistence of the O and R phases in the PPT/MPB-like region.[28,47] In the PPT/MPB-like region, the domain was easy to switch under the external electric field, showing a high spontaneous polarization. Thus, the ferroelectric properties in that region were better than that in a single-phase region of the samples. Moreover, the BCT–BZT ceramics prepared via sintering of BCT and BZT nanoparticles had fewer PNRs and more non-180° domains than those obtained via the conventional method that resulted in the improved ferroelectric properties.[48] However, E_c was only slightly enhanced at x = 0.10, which was due to the restoring force provided by the defect dipole under an external electric field with increasing x values.[49] Moreover, the decreasing tendency of the P_r and E_c values at excessive zirconium contents was attributed to the distortion in the ABO_3 structure.

The piezoelectric constant (d_{33}), electromechanical coupling factor (k_p) and mechanical quality factor (Q_m) of the BCT–BZT ceramics prepared with different zirconium contents (x) are shown in Fig. 9. The d_{33} and k_p values initially increased and then decreased with further addition of zirconium; the maximum values (d_{33} = ~240 pC/N; k_p = 0.22) were obtained close to the PPT/MPB-like region at

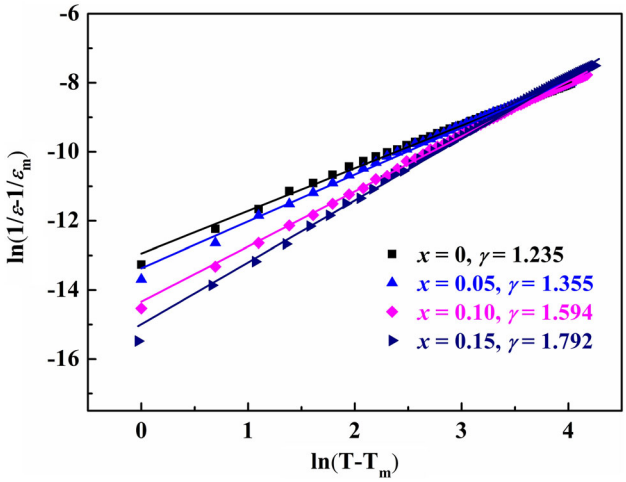

Fig. 7. The plots of $\ln(1/\varepsilon_r - 1/\varepsilon_m)$ versus $\ln(T - T_m)$ at 10 kHz for BCT–BZT ceramics with various zirconium contents (x).

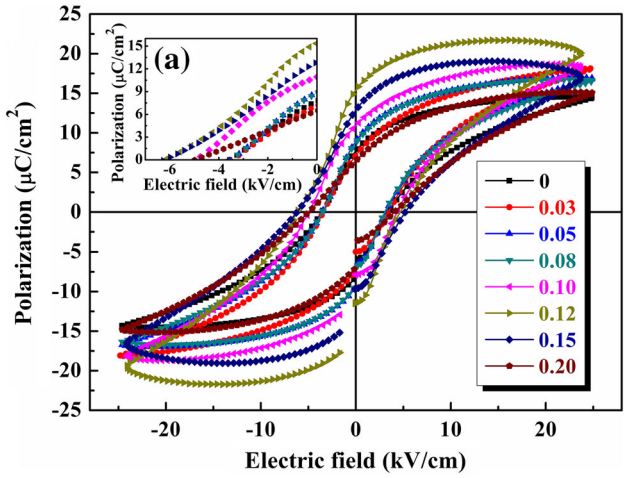

Fig. 8. Polarization versus electric field (P–E) hysteresis loops of BCT–BZT ceramics with various zirconium contents (x). The inset in (a) shows the curves of polarization versus enlarged regions (−7 kV/cm to 0 kV/cm) of electric field.

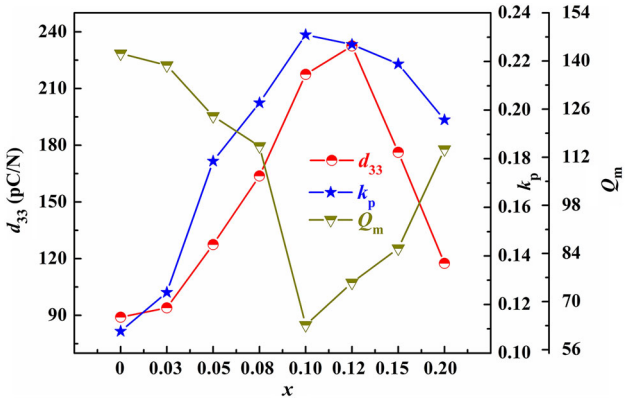

Fig. 9. Piezoelectric constant (d_{33}), electromechanical coupling factors (k_p) and mechanical quality factor (Q_m) of BCT–BZT ceramics with various zirconium contents (x).

x = 0.10, in which polarization could be easily enhanced by an external electric field, resulting in improved piezoelectric properties than that obtained for a single-phase region.[50] However, the piezoelectric properties were lower than those reported in the literature which was attributed to the fine grain size in our study. In addition, Q_m dropped sharply in the PPT/MPB-like region, and this result was associated with the reduced internal strain stress and weak pinching effects in the domain wall.[51]

The relationship between d_{33} and P_r is shown in Eq. 4[41,52]:

$$d_{33} = 2Q_{11} \cdot P_r \cdot \varepsilon_{33}, \quad (4)$$

where Q_{11} is the electrostrictive coefficient and ε_{33} is the dielectric constant. The Q_{11} and ε_{33} values of the BCT–BZT ceramics were comparable to each other under the specified conditions in our study. Thus, d_{33} was proportional to P_r at a certain extent. This observation was consistent with the obtained results discussed above.

CONCLUSIONS

$0.50Ba_{0.9}Ca_{0.1}TiO_3$–$0.50BaTi_{1-x}Zr_xO_3$ (BCT–BZT) lead-free ceramics were prepared via sintering of BCT and BZT nanoparticles at a low temperature of 1260°C. All the BCT–BZT ceramics featured a dense microstructure and a high level of densification under the synthesis conditions employed. XRD analysis revealed the onset of a phase transformation from O to R phase with increasing x values, and the PPT/MPB-like region was observed at x = 0.10. The level of dielectric dispersion, DPT, and relaxor-like ferroelectric characteristics of the ceramics increased with increasing x values, thus showing a strong dependency on the zirconium content. The excellent electrical properties, P_r = 16.4 μC/cm^2, d_{33} = ~240 pC/N, and k_p = 0.22, were detected at the PPT/MPB-like region, thus suggesting that the BCT–BZT ceramics are a promising candidate for application as lead-free ferroelectric ceramics.

ACKNOWLEDGEMENTS

The authors would like to thank the Fundamental Research Funds for National University (CUG120 118), Innovation Program of China University of Geosciences (No. 201310491013), and State Key Laboratory of Advanced Technology for Materials Synthesis Processing (Wuhan University of Technology, 2012-KF-3) for their financial support.

REFERENCES

1. B. Jaffe, W.R. Cook, and H.C. Jaffe, *Piezoelectric Ceramics* (New York: Academic, 1971), pp. 185–212.
2. M.A. Mohiddon, A. Kumar, and K.L. Yadav, *Phys. B* 395, 1 (2007).
3. C.A. Randall, N. Kim, J.P. Kucera, W. Cao, and T.R. Shrout, *J. Am. Ceram. Soc.* 81, 677 (1998).
4. T. Takenaka and H. Nagata, *J. Eur. Ceram. Soc.* 25, 2693 (2005).

5. T.R. Shrout and S.J. Zhang, *J. Electroceram.* 19, 111 (2007).
6. E. Aksel and J.L. Jones, *Sensors* 10, 1935 (2010).
7. R.Z. Zuo, X.S. Fang, and C. Ye, *Appl. Phys. Lett.* 90, 092904 (2007).
8. D. Damjanovic, N. Klein, J. Li, and V. Porokhonskyy, *Funct. Mater. Lett.* 3, 5 (2010).
9. Y. Saito, H. Takao, T. Tani, T. Nonoyama, K. Takatori, T. Homma, T. Nagaya, and M. Nakamura, *Nature* 432, 84 (2004).
10. T. Takenaka, H. Nagata, and Y. Hiruma, *Jpn. J. Appl. Phys.* 47, 3787 (2008).
11. S.O. Leontsev and R.E. Eitel, *Sci. Technol. Adv. Mater.* 11, 044302 (2010).
12. J. Chen, X.L. Chen, F. He, Y.L. Wang, H.F. Zhou, and L. Fang, *J. Electron. Mater.* 43, 1112 (2014).
13. W.F. Liu and X.B. Ren, *Phys. Rev. Lett.* 103, 257602 (2009).
14. T. Maiti, R. Guo, and A.S. Bhalla, *J. Appl. Phys.* 100, 114106 (2006).
15. Y.L. Wang, L.T. Li, J.Q. Qi, and Z.L. Gui, *Ceram. Int.* 28, 657 (2002).
16. Z. Sun, Y. Pu, Z. Dong, Y. Hu, X. Liu, and P. Wang, *J. Mater. Sci.* 25, 1828 (2014).
17. D. Liang, X. Zhu, J. Zhu, J. Zhu, and D. Xiao, *Ceram. Int.* 40, 2585 (2014).
18. W. Liu, W. Chen, L. Yang, L. Zhang, Y. Wang, C. Zhou, S. Li, and X. Ren, *Appl. Phys. Lett.* 89, 172908 (2006).
19. D. Damjanovic, *Appl. Phys. Lett.* 97, 062906 (2010).
20. M.R. Panigrahi and S. Panigrahi, *Phys. B* 405, 2556 (2010).
21. S. Mahajan, O.P. Thakur, D.K. Bhattacharya, and K. Sreenivas, *Mater. Chem. Phys.* 112, 858 (2008).
22. P. Zheng, J.L. Zhang, S.F. Shao, Y.Q. Tan, and C.L. Wang, *Appl. Phys. Lett.* 94, 032902 (2009).
23. P. Wang, Y. Li, and Y. Lu, *J. Eur. Ceram. Soc.* 31, 2005 (2011).
24. Y.S. Tian, Y.S. Gong, Z.L. Zhang, and D.W. Meng, *J. Mater. Sci.* 25, 5467 (2014).
25. S.J. Kuang, X.G. Tang, L.Y. Li, Y.P. Jiang, and Q.X. Liu, *Scripta Mater.* 61, 68 (2009).
26. L. Dong, D.S. Stone, and R.S. Lakes, *J. Appl. Phys.* 111, 084107 (2012).
27. J. Wu, D. Xiao, W. Wu, Q. Chen, J. Zhu, Z. Yang, and J. Wang, *J. Eur. Ceram. Soc.* 32, 891 (2012).
28. S.W. Zhang, H. Zhang, B.P. Zhang, and S. Yang, *J. Alloy. Compd.* 506, 131 (2010).
29. N. Pisitpipathsin, P. Kantha, K. Pengpat, and G. Rujijanagul, *Ceram. Int.* 39, S35 (2013).
30. W. Lin, L. Fan, D. Lin, Q. Zheng, X. Fan, and H. Sun, *Curr. Appl. Phys.* 13, 159 (2013).
31. X. Tang, J. Wang, X. Wang, and H. Chan, *Solid State Commun.* 131, 163 (2004).
32. L. Gao, J.W. Zhai, Y.W. Zhang, and X. Yao, *J. Appl. Phys.* 107, 064105 (2010).
33. S.W. Zhang, H.L. Zhang, B.P. Zhang, and G.L. Zhao, *J. Eur. Ceram. Soc.* 29, 3235 (2009).
34. X.G. Tang and H.L.W. Chan, *J. Appl. Phys.* 97, 034109 (2005).
35. Z. Yu, C. Ang, R. Guo, and A. Bhalla, *Mater. Lett.* 61, 326 (2007).
36. Z. Sun, Y. Pu, Z. Dong, Y. Hu, P. Wang, X. Liu, and Z. Wang, *Mater. Sci. Eng. B* 185, 114 (2014).
37. X. Tang, K.H. Chew, and H. Chan, *Acta Mater.* 52, 5177 (2004).
38. S. Ye, J. Fuh, L. Lu, Y.L. Chang, and J.R. Yang, *RSC Adv.* 3, 20693 (2013).
39. T. Maiti, R. Guo, and A. Bhalla, *J. Am. Ceram. Soc.* 91, 1769 (2008).
40. T. Matthew, *Eur. J. Phys.* 21, 459 (2000).
41. J. Hao, W. Bai, and W. Li, *J. Am. Ceram. Soc.* 95, 1998 (2012).
42. P. Parjansri, S. Eitssayeam, and U. Intatha, (*IEEE*, ISAF/PFM, 2013), pp. 115-118.
43. W.J. Merz, *Phys. Rev.* 77, 52 (1950).
44. P. Zheng, K. Song, H. Qin, L. Zheng, and L. Zheng, *Curr. Appl. Phys.* 13, 1064 (2013).
45. O.P. Thakur, C. Prakash, and A.R. James, *J. Alloy. Compd.* 470, 548 (2009).
46. I. Coondoo, N. Panwar, H. Amorín, M. Alguero, and A.L. Kholkin, *J. Appl. Phys.* 113, 214107 (2013).
47. Y.J. Dai, X.W. Zhang, and K.P. Chen, *Appl. Phys. Lett.* 94, 042905 (2009).
48. N. Ma, B.P. Zhang, W.G. Yang, and D. Guo, *J. Eur. Ceram. Soc.* 32, 1059 (2012).
49. P.F. Zhou, B.P. Zhang, L. Zhao, X.K. Zhao, L.F. Zhu, L.Q. Cheng, and J.F. Li, *Appl. Phys. Let.* 103, 172904 (2013).
50. W. Li, Z. Xu, R. Chu, P. Fu, and G. Zang, *Mater. Lett.* 64, 2325 (2010).
51. M.C. Ehmke, J. Daniels, J. Glaum, M. Hoffman, J.E. Blendell, and K.J. Bowman, *J. Am. Ceram. Soc.* 96, 2913 (2013).
52. M.J. Haun, E. Furman, S.J. Jang, and L.E. Cross, *Ferroelectrics* 99, 13 (1989).